

High resolution spectroscopy of a quantum dot driven bichromatically by two strong fields

Chris Gustin^{†,1,2,*}, Lukas Hanschke^{†,3,4,*}, Katarina Boos^{3,4,*}, Jonathan R. A. Müller^{‡,5}, Malte Kremser^{5,4}, Jonathan J. Finley^{5,4}, Stephen Hughes² and Kai Müller^{3,4}

¹*Department of Applied Physics, Stanford University, Stanford, California 94305, USA*

²*Department of Physics, Engineering Physics, and Astronomy,
Queen's University, Kingston, Ontario K7L 3N6, Canada*

³*Walter Schottky Institut and Department of Electrical and Computer Engineering,
Technische Universität München, 85748 Garching, Germany*

⁴*Munich Center for Quantum Science and Technology (MCQST), Schellingstr. 4, 80799 Munich, Germany*

⁵*Walter Schottky Institut and Physik Department,
Technische Universität München, 85748 Garching, Germany*

(Dated: April 7, 2022)

We present spectroscopic experiments and theory of a quantum dot driven bichromatically by two strong coherent lasers. In particular, we explore the regime where the drive strengths are substantial enough to merit a general non-perturbative analysis, resulting in a rich higher-order Floquet dressed-state energy structure. We present high resolution spectroscopy measurements with a variety of laser detunings performed on a single InGaAs quantum dot, with the resulting features well explained with a time-dependent quantum master equation and Floquet analysis. Notably, driving the quantum dot resonance and one of the subsequent Mollow triplet sidepeaks, we observe the disappearance and subsequent reappearance of the central transition at high detuned-laser pump strengths and additional higher-order effects, e.g. emission triplets at higher harmonics and signatures of higher order Floquet states. For a similar excitation condition but with an off-resonant primary laser, we observe similar spectral features but with an enhanced inherent spectral asymmetry.

I. INTRODUCTION

Semiconductor quantum dots (QDs) provide an excellent solid-state platform for the coherent control of quantum light-matter interactions. In particular, optically-active excitons (electron-hole pairs) can behave as mesoscopic two-level systems, allowing for controlled emission of radiation for various forms of quantum information processing protocols, including the generation of single photons [1–4] and entangled photon pairs [5, 6]. Coherent control of quantum systems via continuous wave or pulsed lasers allows for additional tailoring of the emitted photon spectrum by enabling engineered quantum evolution under strong field interaction, which can manifest in strong-field observables such as the Mollow triplet, Ramsey interference, and Rabi oscillations [7–12].

To provide further control of the dressed-state spectrum, two or more coherent drives can be introduced into the excitation scheme, with potential applications including enhanced phonon reservoir squeezing [13], suppression of the resonant spontaneous emission spectral line (which can overlap with the scattered laser) [14], spectral line narrowing [15], and gain without population inversion [16]. Periodic driving of quantum systems also can suppress decoherence via continuous dynamical decoupling and the coherent destruction of tunneling [17–

19]. The specific case of two-level systems driven by two coherent drives of differing frequencies (bichromatic), initially motivated by amplitude-modulated driving, has been theoretically studied (e.g., see Refs. 20–24), as well as experimentally using QDs [14, 16, 25], atoms [26, 27], and superconducting qubits [28]. Experiments on bichromatically driven QDs have studied certain regimes of two-color excitation (including “doubly dressed” states), and have revealed an interference-based suppression of the spectral emission line resonant with the exciton frequency, when driven with a strong resonant laser and a second laser detuned to one of the sidebands of the resultant Mollow triplet, as well as a multiphoton AC stark shift of subharmonic resonances [14, 29].

In this work, we explore the regime where both laser drives are strong enough to create a significant component of the Hamiltonian which is, even in any rotating frame, periodic in time, resulting in a rich Floquet dressed-state energy structure, where a general non-perturbative analysis is warranted. We provide high resolution spectroscopy measurements, the results of which are well replicated with a time-dependent master equation approach, non-perturbative in the coherent drive strengths with respect to the periodicity of the Hamiltonian, which is conceptually straightforward and can easily be generalized to include, e.g., exciton-phonon interactions. We also elucidate how the manifold of bichromatically dressed states which arise from the time-periodic Hamiltonian can be calculated to arbitrary order in harmonic expansion with a Floquet approach, and show an excellent agreement in the transitions it predicts with the full calculations and experiments. Our

* These authors contributed equally to this manuscript

† cgustin@stanford.edu, lukas.hanschke@wsi.tum.de

‡ present address: Toshiba Research Europe Limited, Cambridge Research Laboratory, Cambridge CB4 0GZ, UK

experiments reveal, for the first time to our knowledge, the higher order effect of the resonant spectral line re-emergence at high detuned-laser pump strengths [23], for the specific excitation scenario of a resonant primary laser and a secondary laser detuned to a Mollow side-peak of the primary laser. We also confirm suppression of spectral lines due to quantum interference and coupling to subharmonic resonances which has already been studied by He *et al.* [14] and observe additional features of the fluorescence spectrum, including the formation of triplets centered at higher multiples of the Rabi energy of the driving laser. Furthermore, by driving the QD under a similar excitation scenario but with an off-resonant primary laser, we observe similar spectral features as the resonant case but with heightened inherent spectral asymmetry, in contrast to the (pure dephasing free) monochromatic case [30].

The rest of this paper is organized as follows: in Sec. II we outline the theory of our time-dependent master equation approach, as well as the semi-analytical Floquet method for calculating the position of potential spectral lines. We describe our high resolution spectroscopy measurements in Sec. III, and detail the experimental and theoretical results in Sec. IV. In Sec. V we conclude. We also include two appendices: in Appendix A, we provide additional detail on the calculation of the Floquet resonances, and in Appendix B we provide single drive experiments and extract from them an estimate of the phonon coupling strength, which allow us to verify that electron-phonon coupling is qualitatively insignificant in the bichromatic driving regimes studied in the main text.

II. THEORY

We first provide the theory of bichromatic driving in the strong field regime, using (A) a quantum master equation with a time-dependent drive, and (B) a semi-analytical Floquet theory analysis to identify the time-dependent eigenstates of the Hamiltonian.

A. Quantum master equation and incoherent spectra

We model a bichromatically driven QD as a two-level system, with ground $|g\rangle$ and exciton $|x\rangle$ states. The QD is coherently driven by two lasers at frequencies ω_1 and ω_2 , treated semiclassically, with Rabi energies Ω_1 and Ω_2 , respectively. The first laser is detuned from the exciton frequency (ω_x) by $\Delta_1 = \omega_x - \omega_1$, and the second laser is detuned by $\Delta_2 = \omega_x - \omega_2$. After making the rotating-wave approximation with respect to the dipole-field interaction term, our system Hamiltonian is periodic with frequency $\Delta = \Delta_1 - \Delta_2 = \omega_2 - \omega_1$, and in a frame rotating at ω_1 , is (letting $\hbar = 1$ throughout)

$$H(t) = \Delta_1 \sigma^+ \sigma^- + \frac{1}{2} \left[(\Omega_1 + \Omega_2 e^{-i\Delta t}) \sigma^+ + \text{H.c.} \right], \quad (1)$$

with the Pauli operators $\sigma^- = |g\rangle \langle x|$, $\sigma^+ = |x\rangle \langle g|$. For QDs, our two-level approximation is justified if we assume the detunings to be small enough as to be far off from any resonances involving multi-exciton states – a requirement easily satisfied here. For convenience, we also define the ratio of Rabi energies as $\alpha_c = \Omega_2/\Omega_1$.

We incorporate spontaneous emission at rate γ into the model with an open-system Lindblad master equation for the density operator ρ :

$$\frac{d\rho}{dt} = -i[H(t), \rho] + \frac{\gamma}{2} \mathcal{L}[\sigma^-] \rho + \frac{\gamma'}{2} \mathcal{L}[\sigma^+ \sigma^-] \rho, \quad (2)$$

where $\mathcal{L}[A]\rho = 2A\rho A^\dagger - A^\dagger A\rho - \rho A^\dagger A$; we have also included a phenomenological pure dephasing rate γ' , to capture linewidth broadening, as well as effects including charge noise [31], and, notably, electron-phonon coupling. While electron-phonon scattering has important effects on the dynamics of optically excited QDs [32–38], for the drive strengths and detunings considered in this work, these effects are small and can be accurately approximated at low temperatures as a pure dephasing rate. Considering the simple case of a single laser drive on resonance with the exciton, this rate is approximately [39],

$$\gamma'_{\text{ph}} \approx \pi k_B T \alpha \Omega^2, \quad (3)$$

where α is the phonon coupling strength, k_B is Boltzmann's constant, and T is the temperature. Even at the relatively high drive strength of $\Omega = 100 \mu\text{eV}$, for a phonon coupling rate of $\alpha \lesssim 0.1 \text{ ps}^2$ (which is extracted from single drive measurements as shown in Appendix B), and temperature $T = 4.2 \text{ K}$, this pure dephasing rate $\gamma'_{\text{ph}} \lesssim 2.7 \mu\text{eV}$ is similar to what could be expected from other background dephasing sources, and thus we can neglect phonon coupling beyond this phenomenological treatment for this work (which we have verified numerically by comparing with a full time-dependent polaron-transform model [40, 41]).

We calculate the emitted *incoherent* resonance fluorescence spectrum from the QD in terms of the two-time correlation function:

$$S_i(\omega) = \text{Re} \left[\int_0^\infty d\tau e^{i(\omega - \omega_1)\tau} \int_0^\infty dt \langle \sigma_\delta^+(t) \sigma_\delta^-(t + \tau) \rangle \right], \quad (4)$$

where $\sigma_\delta^\pm = \sigma^\pm - \langle \sigma^\pm \rangle$. As the bichromatically driven system dynamics continually oscillate, the two-time correlation function must be time-averaged over t , for at least the periodicity of the Hamiltonian, $2\pi/|\Delta|$. Furthermore, this should be done in the steady-state condition, namely once any transient phenomena have decayed to zero (i.e., for $t \gg 1/\gamma$). Also note that the integration period of the τ -integral is determined not by the periodicity of the Hamiltonian, but by the decay time of the two-level system. To make this calculation more manageable and/or obtain analytical results, incoherent spectra for bichromatically driven systems have historically typically been calculated using Floquet expansions [14, 16, 20, 21, 25]; however, we calculate the

full correlation function from the master equation solution via the quantum regression theorem, and average directly over t , which is more computationally intensive but has the benefit of simplicity and avoids some of the subtleties involved with averaging over expansions of correlation functions [42].

B. Floquet Theory Analysis

In addition to the full numerical calculation of the resonance fluorescence spectrum with the quantum master equation, it is also useful to extract the doubly dressed states of the system (the frequencies of which determine the spectral lines seen in the spectrum) by calculation of the Floquet energies of the periodic Hamiltonian (1) (see Ref. 43). By exploiting the discrete time-translational symmetry of the Hamiltonian $H(t + nT) = H(t)$ for $n \in \mathbb{Z}$, where $T = 2\pi/|\Delta|$, we construct a simple unitary Floquet model which neglects dissipation to identify the resonances of the system.

For the general time-dependent problem $i \frac{d}{dt} |\psi\rangle = H(t) |\psi\rangle$, the solution is given formally by $|\psi(t)\rangle = U(t, t_0) |\psi(t_0)\rangle$, where $U(t, t_0) = \hat{\tau} \exp\left(-i \int_{t_0}^t H(t') dt'\right)$ and $\hat{\tau}$ is the time-ordering operator. The essential utility of Floquet theory is the transformation of this time-dependent problem to a time-independent one given by an infinite matrix deduced by Fourier expansion of $|\psi(t)\rangle$. This result is possible by Floquet's theorem [44, 45], which states that there exists a complete set of states $|\psi_\lambda(t)\rangle$ indexed by λ that satisfy

$$|\psi_\lambda(t)\rangle = e^{-i\epsilon_\lambda t} |\phi_\lambda(t)\rangle, \quad (5)$$

where ϵ_λ denotes a real Floquet quasienergy, and $|\phi_\lambda(t)\rangle$ has periodicity T . This immediately yields the eigenvalue problem:

$$H_F |\phi_\lambda\rangle = \epsilon_\lambda |\phi_\lambda\rangle, \quad (6)$$

with the Floquet Hamiltonian operator $H_F = H(t) - i \frac{d}{dt}$. Although time-dependent, the Floquet states $|\phi_\lambda(t)\rangle$ form a complete basis for any value of t , and as such the general solution to the Schrödinger equation can be given as

$$|\psi(t)\rangle = \sum_\lambda c_\lambda e^{-i\epsilon_\lambda t} |\phi_\lambda(t)\rangle, \quad (7)$$

where the c_λ are time-independent complex coefficients. As the states $|\phi_\lambda\rangle$ are periodic, Eq. (7) suggests that energies in Floquet systems are only conserved modulo Δ , and it can be shown the transition resonances of the system occur at differences between Floquet energies [44, 45].

For our two-level model, we can expand $|\phi_\lambda\rangle = c_{g,\lambda}(t) |g\rangle + c_{x,\lambda}(t) |x\rangle$, where $c_{g,\lambda}(t)$ and $c_{x,\lambda}(t)$ are periodic with period T . We expand them as Fourier series,

$c(t) = \sum_{m=-\infty}^{\infty} c^{(m)} e^{im\Delta t}$, where m is an integer, and insert the result into Eq. (6):

$$\sum_{m=-\infty}^{\infty} \sum_{\beta=g,x} (H_F - \epsilon_\lambda) c_{\beta,\lambda}^{(m)} e^{im\Delta t} |\beta\rangle = 0. \quad (8)$$

Taking the inner product with $\langle\alpha|$,

$$\sum_{m,\beta} \left[H_{\alpha,\beta} + m\Delta \delta_{\alpha,\beta} \right] c_{\beta,\lambda}^{(m)} e^{im\Delta t} = \sum_m \epsilon_\lambda c_{\alpha,\lambda}^{(m)} e^{im\Delta t}, \quad (9)$$

with $H_{\alpha,\beta} = H_{\alpha,\beta}(t) = \langle\alpha| H(t) |\beta\rangle$. Multiplying by $e^{-in\Delta t}/T$, where n is an integer, and integrating from 0 to T , then

$$\sum_{m,\beta} \left[\frac{1}{T} \int_0^T dt H_{\alpha,\beta} e^{i(m-n)\Delta t} + n\Delta \delta_{\alpha,\beta} \delta_{m,n} \right] c_{\beta,\lambda}^{(m)} = \epsilon_\lambda c_{\alpha,\lambda}^{(n)}. \quad (10)$$

Equation (10) is an eigenvalue equation for the eigenvector of Fourier coefficients $c_{\alpha,\lambda}^{(n)}$ and eigenvalue ϵ_λ , with matrix elements specified by the row indexed by (α, n) and column indexed by (β, m) , and equal to the quantity in square brackets—the matrix representation of H_F . This matrix can be realized computationally by truncating the number of integers n, m considered, and letting each combination of (n, m) correspond to a 2-by-2 block of elements corresponding to the matrix elements of the two-level Hilbert space Hamiltonian, plus $n\Delta$ on the diagonal elements; for more information, see Appendix A. To extract the frequencies of the spectral lines that show up in the emitted spectrum, the eigenvalues of Eq. (10) can be found numerically for a given truncation of integers n, m , and the potential transitions are given by the Floquet-dressed resonant frequencies $\tilde{\omega}_{\lambda,\lambda'} = \omega_1 + (\epsilon_\lambda - \epsilon_{\lambda'})$, where $\lambda \in \{1, 2, \dots, M\}$, and $M = 2(2N + 1)$. Here, N is the order of the harmonics considered in the Floquet matrix (i.e. $n, m = 0, \pm 1, \dots, \pm N$). Thus, considering up to order N yields M^2 potential transitions, although not all these transitions need be driven, and thus may not all show up in the spectrum. Many will also be degenerate. Increasing the Floquet order increases the accuracy of the locations of the spectral lines, as well as increasing the amount of spectral resonances that can be identified.

III. EXPERIMENTS

Experimentally, we performed measurements on InGaAs QDs grown via molecular beam epitaxy with the Stranski-Krastanov mode in a GaAs matrix. We include 17 pairs of alternating GaAs/AlAs layers forming a distributed Bragg reflector below the QD layer to increase the extraction efficiency of the emitted photons. An embedded n -doped GaAs layer 35 nm below the quantum dots forms a Schottky diode together with a semi-transparent 5 nm thick titanium layer evaporated on the

surface of the sample. By applying an external voltage the resulting electric field in the vicinity of the QDs reduces the charge noise. Furthermore, it allows us to deterministically charge the QD and tune the transition of interest in perfect resonance with the excitation laser via the quantum confined Stark effect [46, 47].

The measurements are performed at 4.2 K in a dip stick setup with a confocal microscope, while cross-polarized filtering allows resonant excitation by suppressing the scattered laser in the detection path [48]. To avoid the influence of higher excited states, we investigate the negatively charged exciton transition which lacks a fine structure splitting compared to the neutral exciton transition [49], while higher excited states involve the p -shell states which are several tens of meV detuned. For the high resolution spectroscopy of the dressed states, we employ a scanning Fabry-Pérot cavity with a free spectral range of 30 GHz (124 μeV) and a resolution of 300 MHz (1.24 μeV) where the transmitted signal is recorded with an APD. The exciton resonance of the investigated QD is at $\omega_x = 1362.04$ meV, with a lifetime of 455 ps (decay rate 1.44 μeV).

IV. RESULTS

In Fig. 1, we plot the theoretically calculated emission spectrum from the bichromatically driven QD, where one laser is held fixed on resonance (with the QD exciton), and the other is detuned to the frequency of the lower energy peak of the resulting Mollow triplet. We also show here the transitions predicted by the Floquet theory overlaid on top, showing excellent agreement with the full numerical calculations of the master equation. The potential Floquet transitions are shown for both $N = 1$ and $N = 3$ (which is the lowest integer required to see full agreement with the exact numerical solution), highlighting the higher-order perturbative nature of this pumping regime with respect to $\alpha_c = \Omega_2/\Omega_1$, as well as the rich complexity of the Floquet eigenstructure. This excitation condition, for small α_c , gives rise to “doubly-dressed states”; for low values of α_c , each of the Mollow triplet peaks at ω_1 , $\omega_1 \pm \Omega_1$ are split by approximately $\pm\Omega_2$, creating eight total peaks (the center line being suppressed) [27]. As Ω_2 is increased with Ω_1 held fixed, the center transition line disappears due to destructive interference from transition amplitudes [14] and subsequently reappears at higher secondary laser strengths with transition probability having a leading term fourth order in α_c [23]. Additionally, higher order (in α_c) effects lead to additional triplets forming at integer multiples of Ω_1 from the center exciton frequency [23]. Specifically, the leading order transition probabilities for transitions occurring at triplets centered at $\omega = \omega_1 \pm n\Omega_1$, where n is an integer greater than 1, scale with $\alpha_c^{2(n-1)}$ [23]. This can be understood as a nonlinear multiphoton effect *between* the two detuned driving fields and the exciton. In contrast to analytical calculations perturbative with respect

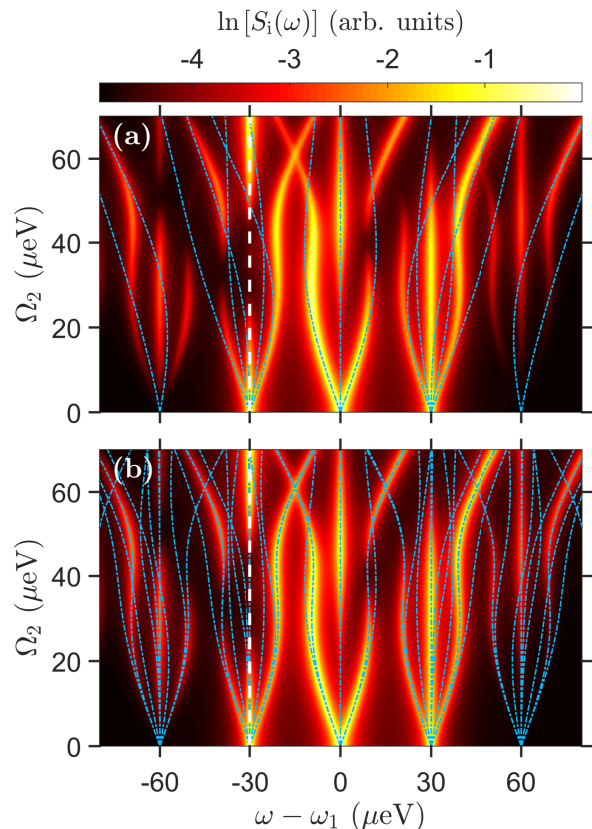


FIG. 1. Theoretical spectrum (plotted on a logarithmic scale for clarity), with $\gamma = \gamma' = 1$ μeV , $\Omega_1 = 30$ μeV , $\Delta_1 = 0$, $\Delta_2 = 30$ μeV . Floquet transitions up to order (a) $N = 1$ and (b) $N = 3$ (the minimum number to see complete agreement with the observed spectral lines). The color scheme is modified to enhance the visibility of the Floquet resonances, and the location of the second laser at ω_2 is shown as a white vertical dashed line.

to α_c [23], which predict a symmetric spectrum about $\omega = \omega_1$, our results show the inherent asymmetry in the spectrum, even for $\alpha_c < 1$, and we note this asymmetry persists even if we take $\gamma' = 0$. For $\alpha_c > 1$, the structure of this excitation condition changes; it is preferable to not consider this system as a second laser doubly-dressing a Mollow sidepeak, but rather as an off-resonant Mollow triplet centered at $\omega = \omega_2$, dressed by a weaker resonant laser.

Figure 2 shows the theoretical and experimental emission spectra for the same scenario of one resonant laser plus a second with frequency resonant to the Rabi sidepeak induced by the first laser. Here both a red-detuned and a blue-detuned second laser are considered. Note that, in the theoretical spectrum, flipping the sign of Δ is formally equivalent to a sign change in $\omega - \omega_1$ (mirroring the spectrum) for this master equation; by considering Eq.’s (2) and (4) and using the quantum regression theorem, it can be shown that $\Delta \rightarrow -\Delta$ is equivalent to $\langle \sigma_\delta^+(t)\sigma_\delta^-(t+\tau) \rangle \rightarrow \langle \sigma_\delta^+(t)\sigma_\delta^-(t+\tau) \rangle^*$, which has the same effect in Eq. (4) as taking $\omega - \omega_1 \rightarrow -(\omega - \omega_1)$.

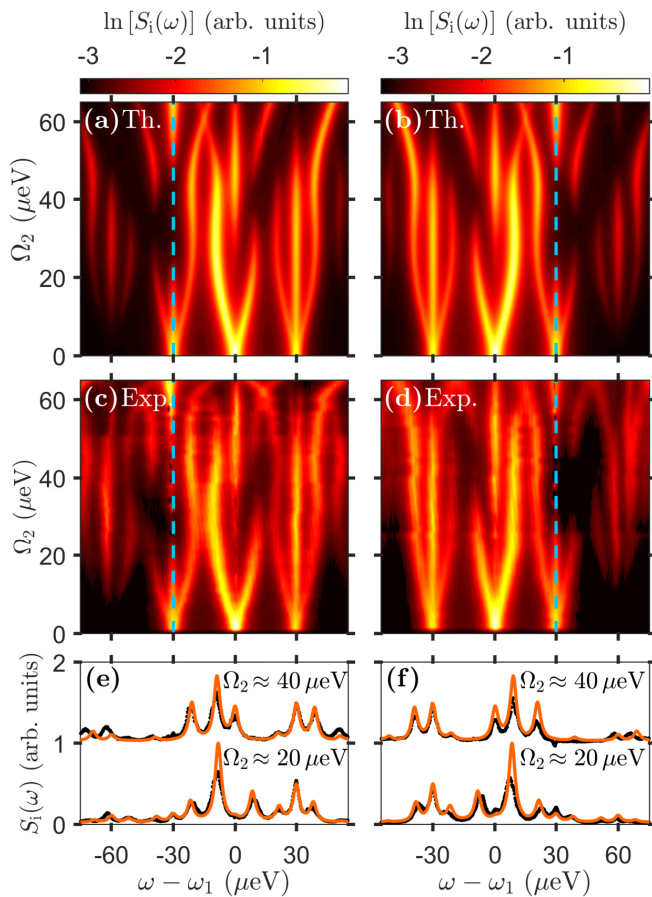


FIG. 2. Emission spectrum of a QD dressed by a resonant ($\Delta_1 = 0$) laser with drive strength $\Omega_1 = 30 \mu\text{eV}$, as well as a second laser with detuning $\Delta_2 = -\Delta = 30 \mu\text{eV}$ for (a,c), and $\Delta_2 = -30 \mu\text{eV}$ for (b,d), and varying drive strength Ω_2 . (a,b) show the theoretical calculation with $\gamma = 1.66 \mu\text{eV}$ and $\gamma' = 2 \mu\text{eV}$, and (c,d) are experimental data. The location of the second laser at ω_2 is shown as a blue vertical dashed line. (e) and (f) give the data (black) and simulation (orange) for specific values of Ω_2 for (a,c) and (b,d), respectively. At the far ends of the spectra, the Fabry-Pérot setup leads to a replication of spectral lines separated by the free spectral range.

We observe, in both theory and experiment, the disappearance and subsequent reappearance of the center (at $\omega = \omega_1$) resonance fluorescence transition line as a function of secondary drive power Ω_2 — a higher order effect in α_c . The additional triplets centered at plus (minus) twice the Rabi energy Ω_1 for a blue (red) detuned second laser resulting from higher order effects are also clearly visible in the experimental and theoretical spectra. They are most pronounced for equal Rabi energies of both lasers. Note that we have made no specific effort to fit the decay and pure dephasing rates γ, γ' to match experiment. Anomalously, we observe a crossing of spectral lines at $\omega - \omega_1 \approx 15 \mu\text{eV}$ in (c), and $\omega - \omega_1 \approx -15 \mu\text{eV}$ in (d), which correspond to Floquet transitions in our models, but are not reproduced by the full calculations.

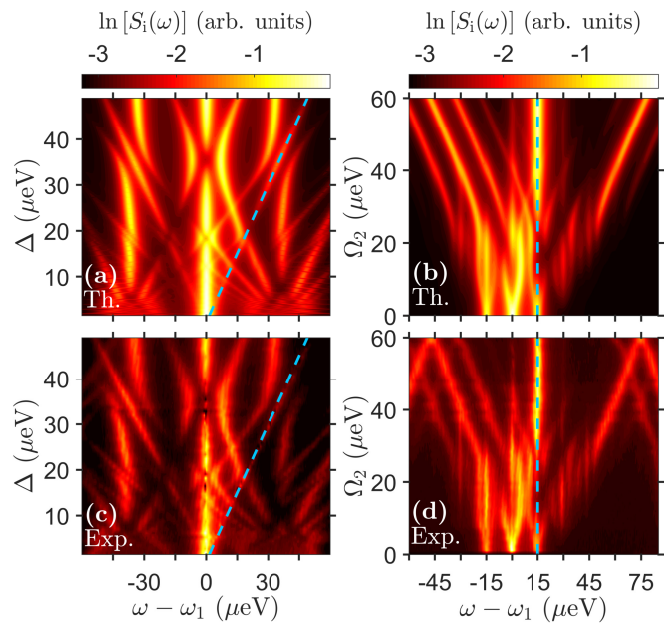


FIG. 3. (a,c) Theoretical and experimental log-scale spectra of a QD dressed by a resonant ($\Delta_1 = 0$) laser with fixed drive strengths (for the simulated spectra, $\Omega_1 = 35 \mu\text{eV}$ and $\Omega_2 = 15 \mu\text{eV}$), where the detuning of the second laser $\Delta = -\Delta_2 = \omega_2 - \omega_1$ is varied. (b,d) Theoretical and experimental spectra of a QD dressed by resonant drive $\Omega_1 = 15 \mu\text{eV}$, with the second laser detuned $\Delta = 15 \mu\text{eV}$ and allowed to vary in strength, revealing a Mollow triplet forming centered at $\omega - \omega_2$ for $\Omega_2 \gg \Omega_1$. For both theoretical calculations, $\gamma = 1.66 \mu\text{eV}$, and $\gamma' = 2 \mu\text{eV}$. The location of the second laser at ω_2 is shown as a thin blue dashed line. In (d), the Fabry-Pérot setup leads to a replication of spectral lines separated by the free spectral range, seen in the regions $\omega - \omega_1 < -45 \mu\text{eV}$, and $\omega - \omega_1 > 75 \mu\text{eV}$.

In Fig. 3(a,c), we plot the theoretical and experimental emission spectra for fixed drive strengths, with the first laser resonant and varying detuning of the second laser. In agreement with measurements by He *et al.*, [14] we observe suppression of the central transition when the second laser is in resonance with the sideband of the Mollow triplet at $\Delta = 35 \mu\text{eV}$ or one of its subharmonics Ω_1/n for integer n up to 3. This process can be associated with destructive quantum interference for the case where the second laser is resonant with the sideband, or a multiphoton quantum interference for the resonance with a subharmonic [14, 23, 29]. Here, the second laser can couple via n photons to the system. In addition to suppression of spectral transitions, a series of triplets evolves separated by Ω_1/n . For the first subharmonic $n = 2$ at $\Delta \approx 17.5 \mu\text{eV}$, a doublet at the center, a triplet at the low energy side and two at higher energies are visible. The second subharmonic resonance $n = 3$ at $\Delta \approx 11.7 \mu\text{eV}$ is not as pronounced, but a similar spectrum is observable. In the limit $\Delta = \Delta_2 = 0$, besides their drive strengths, both lasers are only distinguishable by their relative phase, resulting in a modified Mollow

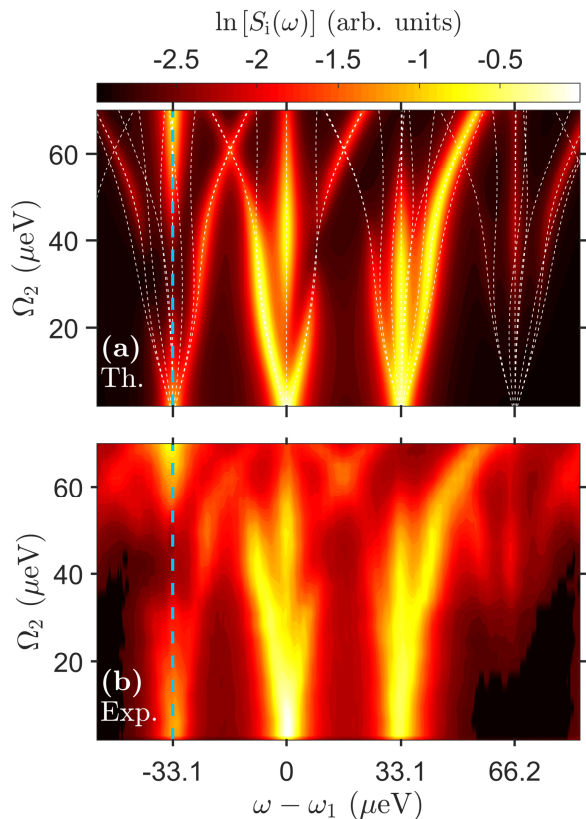


FIG. 4. Theoretical and experimental log-scale spectra of a QD dressed by a primary laser with strength $\Omega_1 = 31.6 \mu\text{eV}$ and (red) detuning $\Delta_1 = 10 \mu\text{eV}$, and a second laser with varied power dressing the red sideband ($\Delta = -\sqrt{\Omega_1^2 + \Delta_1^2}$). The locations of potential Floquet transitions are faintly overlaid in (a) as dashed white lines, and we use $\gamma = 1.66 \mu\text{eV}$, and $\gamma' = 2 \mu\text{eV}$. The location of the second laser at ω_2 is shown as a blue vertical dashed line.

triplet with plateau-like sidebands [14].

To investigate a wider regime of the bichromatically excited QD, we also look at the case of a sideband dressed by the second laser again, while the first laser remains resonant with the exciton transition (Fig. 3 (b,d)). With an initially smaller Rabi energy of $\Omega_1 = 15 \mu\text{eV}$, we allow the drive strength to increase into the regime where $\alpha_c \gg 1$. For the case where both lasers have similar strength $\Omega_1 \approx \Omega_2$ the same features as in Fig. 2 are observable. As a wider range of the spectrum is analysed here, triplets at higher multiples of the Rabi energy $\Omega_1 \times m$ are visible in both theoretical and experimental spectra. They are centered at $m = -2, 2, 3$. So far, only one emission triplet at twice the Rabi energy has been observed, in a bichromatically driven atom [27]. For stronger drive strength of the second laser, the transition back to the Mollow excitation regime can be seen, where a dominant triplet begins to form centered around the second laser frequency ω_2 ; the sidebands shift linearly away from $\omega = \omega_2$ with increasing drive strength Ω_2 .

In Fig. 4, we plot the theoretical and experimental

emission spectra for a detuned primary laser ($\Delta_1 = 10 \mu\text{eV}$), where again the second laser dresses the sidepeak. As expected, with increasing drive strength of the second laser, similar spectra compared to the resonant scenario are observed, while the asymmetry for small α_c is increased. In contrast to the single drive off-resonant Mollow triplet, which is symmetrical in the absence of pure dephasing, there is a strong inherent asymmetry in the Mollow-like spectrum for small but nonzero α_c , which persists in our simulations even with $\gamma' = 0$ (not shown) [30]. While dephasing generically broadens spectral peaks, it will also in general affect the relative spectral weights of differing peaks; pure dephasing in a bare-state basis appears as non-radiative dissipation when viewed in the system (Floquet) eigenbasis, which can violate the principle of detailed balance and thus generically changes the distribution of spectral weights (peak areas) [30]. Specifically, for the regimes studied in this work, we do find in our simulations that dephasing will slightly change the distribution of spectral weights, but this effect is generally insignificant to qualitatively affect our plots, and largely serves to broaden the spectral linewidths.

V. CONCLUSIONS

In conclusion, we have presented high resolution spectroscopy measurements of a single QD dressed simultaneously by two coherent laser drives in general non-perturbative regimes with respect to the laser drive strengths and detunings. These measurements are reproduced with excellent accuracy by a master equation model of a time-dependent Lindblad master equation which can be easily generalized to incorporate different environmental couplings (e.g., cavity, phonon scattering). The transition lines are identifiable using semi-analytic Floquet theory, with higher order harmonics required for accurate location of the spectral lines, which is indicative of the regime with two strong components of the bichromatic field.

For the excitation scenario of one laser resonant with the QD, and one resonant to a sidepeak of the resulting Mollow triplet, further evidence of the regime of excitation with two strong fields can be seen in the formation of additional spectral triplets at two and three times the central laser Rabi energy, the disappearance and subsequent re-emergence of the central spectral peak, and the transition to a detuned Mollow triplet centered around the second laser as its drive strength is increased well beyond the first laser strength. We also have considered a similar excitation scenario, but with both lasers off-resonant, and observed an enhanced inherent spectral asymmetry relative to the resonant primary laser case, in contrast to the monochromatic case where the spectrum is completely symmetric in the absence of additional dephasing mechanisms. All of these features are very well reproduced by theoretical calculations. These

results reveal broad potential for spectral engineering using Floquet Hamiltonians (multi-color coherent excitation) which is highly general and rich in structure and optical physics.

ACKNOWLEDGMENTS

We acknowledge funding from Queen's University, the Canadian Foundation for Innovation, the Natural Sciences and Engineering Research Council of Canada, the European Unions Horizon 2020 research and innovation programme under grant agreement No. 820423 (S2QUIP), the German Federal Ministry of Education and Research via the funding program Photonics Research Germany (contract number 13N14846) and the Deutsche Forschungsgemeinschaft (DFG, German Research Foundation) under Germany's Excellence Strategy EXC-2111 390814868. KM acknowledges support from the Bavarian Academy of Sciences and Humanities.

Appendix A: Matrix Representation of H_F

Here we show explicitly how the eigenvalues can be extracted from the matrix representation of H_F to a certain harmonic order. For example, if we consider transitions up to order $N = 1$ in the harmonic expansion, we can represent H_F from Eq. (10) in the basis $(1, 0, -1)$:

$$H_F = \begin{bmatrix} \mathbf{M}_{1,1} & \mathbf{M}_{1,0} & \mathbf{0} \\ \mathbf{M}_{1,0}^\dagger & \mathbf{M}_{0,0} & \mathbf{M}_{1,0} \\ \mathbf{0} & \mathbf{M}_{1,0}^\dagger & \mathbf{M}_{-1,-1} \end{bmatrix}, \quad (\text{A1})$$

where we let bold denote 2-by-2 matrices in the two-level system basis (x, g) , and we have made use of the fact that, clearly, $\mathbf{M}_{n,m} = \mathbf{M}_{m,n}^\dagger$, and $\mathbf{M}_{m,m\mp 1} = \mathbf{M}_{m\pm 1,m}$. Furthermore, elements with $|n - m| > 1$ vanish due to the form of the Hamiltonian in Eq. (1). Evaluating the matrix elements explicitly, to order $N = 1$, then

$$H_F = \frac{1}{T} \int_0^T dt \begin{bmatrix} \mathbf{H} + \Delta \mathbf{1} & \mathbf{H} e^{-i\Delta t} & \mathbf{0} \\ \mathbf{H} e^{i\Delta t} & \mathbf{H} & \mathbf{H} e^{-i\Delta t} \\ \mathbf{0} & \mathbf{H} e^{i\Delta t} & \mathbf{H} - \Delta \mathbf{1} \end{bmatrix}$$

$$= \frac{1}{2} \begin{bmatrix} 2(\Delta_1 + \Delta) & \Omega_1 & 0 & 0 & 0 & 0 \\ \Omega_1 & 2\Delta & \Omega_2 & 0 & 0 & 0 \\ 0 & \Omega_2 & 2\Delta_1 & \Omega_1 & 0 & 0 \\ 0 & 0 & \Omega_1 & 0 & \Omega_2 & 0 \\ 0 & 0 & 0 & \Omega_2 & 2(\Delta_1 - \Delta) & \Omega_1 \\ 0 & 0 & 0 & 0 & \Omega_1 & -2\Delta \end{bmatrix}, \quad (\text{A2})$$

the eigenvalues of which give the energy spectrum of the field-dressed Floquet states in the frame of the exciton (to harmonic order $N = 1$).

Appendix B: Resonance Fluorescence under a Single Strong Drive

To determine the regime in which pump-induced electron-phonon interactions become significant, we study the resonance fluorescence spectrum of a QD driven by a single resonant coherent drive, where the drive strengths are large enough to enter a regime in which electron-phonon scattering is appreciable. For theoretical calculations, we use the polaron transform model from Ref. [41], with a time-independent resonant drive on a two-level system without a cavity mode. The phonon scattering is characterized by the phonon spectral function $J(\omega) = \alpha \omega^3 \exp\left[-\frac{\omega^2}{2\omega_b^2}\right]$, with phonon coupling strength α and phonon cutoff frequency ω_b . We let $\omega_b = 0.9$ meV, consistent with previous experiments [50]. By curve fitting the data of Fig. 5 (described below) with reference to Eq. (3), we find parameters $\alpha = 0.1$ ps² and $\gamma' = 10$ μ eV. Eq. (4) remains valid for calculation of the incoherent spectrum, but the t -integral becomes trivial in the steady state condition. We use a decay rate of $\gamma = 1.66$ μ eV. Note that here we include the full phonon sideband that arises from the polaron solution [51]. To account for heating of the QD sample induced by the large drive strengths, which results in an exciton resonant frequency shift in the experimental data, we sweep the laser detuning to find the resonant condition for each of the power-dependent measurements.

Under resonant excitation, the incoherent resonance fluorescence spectrum exhibits the well-known Mollow triplet shape, and by curve fitting to Lorentzian functions (for $\Omega' \gg \gamma, \gamma'$, where Ω' denotes the polaron-renormalized Rabi energy [41], such that the peaks are separated and well-represented by Lorentzians), we extract values of the full width(s) at half maximum (FWHM) and spectral weight. In Fig. 5(a), we plot the fitted FWHM for the Mollow sidepeaks as a function of the square of the drive amplitude. The parameters $\alpha = 0.1$ ps² and $\gamma' = 10$ μ eV were found by curve fitting to Eq. (3) (with $\Omega \rightarrow \Omega'$) with an additional offset determined by γ' ; note that here we are simply using γ' as a crude substitute for peak broadening that occurs over long timescales — we use a much smaller value in the main text as pure dephasing in the general case should correspond to processes that occur on the timescales of the excitation dynamics. As one can not rule out other dephasing processes, which scale with the laser power, we can be precise by saying these measurements suggest $\alpha \lesssim 0.1$ ps². Indeed the difference in the theoretical red and blue curves (which is minimal in the experimental data) is much less visible for smaller values of α (e.g., $\alpha = 0.06$ ps², consistent with Ref. [50]), indicating this is likely the case.

In Fig. 5(b), we plot the ratio of red and blue Mollow sidebands as a function of drive amplitude. Our simulations (not shown) reveal that the sideband ratio is nearly independent of phonon parameters α and ω_b ,

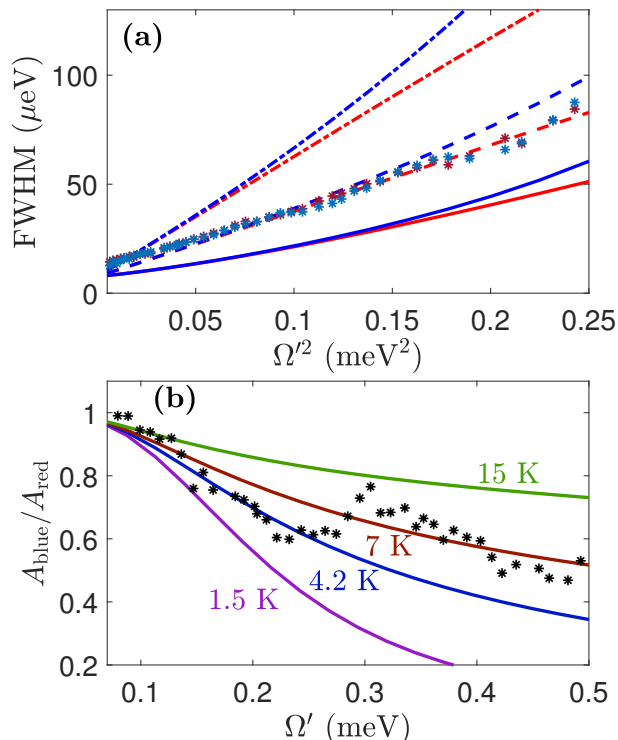


FIG. 5. (a) Fitted FWHM of red (shown as red) and blue (shown as blue) Mollow sidepeaks for experimental data (points), and theoretical curves at temperatures $T = 7\text{ K}$ (dash-dotted lines), $T = 4.2\text{ K}$ (dashed lines), and $T = 1.5\text{ K}$ (solid lines). (b) Ratio of the integrated intensities of blue and red detuned sidebands as a function of the Rabi energy. Experimental data shown as black points, and theoretical curves are given for various temperatures.

with the vast majority of its dependency coming from the temperature. This is understood by recalling that temperature is what determines the amount of phonons available in the thermal bath, which is the origin of this

asymmetry. Making a direct comparison of experiment and theory is complicated because of the bump in the experimental data at $\Omega' \approx 0.3\text{ meV}$, which may be due to confined phonon effects [50], and because the high laser powers used in these single-drive experiments are large enough to induce heating in the sample, resulting in a power-dependent temperature. However, by analysis of the slope of the data, the effective temperatures can be constrained to $T \lesssim 7\text{ K}$, with the theoretical curve at $T = 4.2\text{ K}$ being in excellent agreement with experimental data for small values of Ω' . Note that if we use $\alpha \sim 0.05\text{ ps}^2$, the experimental data of the ratio of the sidepeaks as a function of drive strength lines up much more closely with the $T = 1.5\text{ K}$ curve, indicating that $0.05\text{ ps}^2 \lesssim \alpha \lesssim 0.1\text{ ps}^2$, in accordance with our discussion of Fig. 5(a). Note that we have not fitted the phonon cutoff frequency ω_b , but this parameter does not enter into the low-drive dephasing rate in Eq. (3) and thus has a smaller influence in this regime, and as well it is constrained by the size of the QD.

Comparison of theory and experiment for both these plots suggests that a temperature of between $T = 4.2\text{ K}$ and $T = 7\text{ K}$ gives the closest agreement between the two results. Although in absence of a drive the sample is measured to be at $T = 4.2\text{ K}$, the strong laser powers in these measurements cause a power-dependent heating which is not observably present for the bichromatic measurements. Thus, these results suggest that a polaron transform phonon model at $T = 4.2\text{ K}$, using $\alpha \lesssim 0.1\text{ ps}^2$ is very likely appropriate for the main results of this paper. As discussed in Sec. II, these parameters are expected to give negligible phonon effects (beyond pure dephasing) for the strengths of the bichromatic drives used in this work, further justifying the phenomenological pure-dephasing treatment of the electron-phonon interaction. Note that without any phonon coupling in the simulations, the functions in these plots become trivially identically equal to one.

[1] T. Grange, N. Somaschi, C. Antón, L. De Santis, G. Coppola, V. Giesz, A. Lemaître, I. Sagnes, A. Auffèves, and P. Senellart, “Reducing Phonon-Induced Decoherence in Solid-State Single-Photon Sources with Cavity Quantum Electrodynamics,” *Phys. Rev. Lett.* **118**, 253602 (2017).
[2] X. Ding, Y. He, Z.-C. Duan, N. Gregersen, M.-C. Chen, S. Unsleber, S. Maier, C. Schneider, M. Kamp, S. Höfling, C.-Y. Lu, and J.-W. Pan, “On-Demand Single Photons with High Extraction Efficiency and Near-Unity Indistinguishability from a Resonantly Driven Quantum Dot in a Micropillar,” *Phys. Rev. Lett.* **116**, 020401 (2016).
[3] P. Senellart, G. Solomon, and A. White, “High-performance semiconductor quantum-dot single-photon sources,” *Nat. Nanotech.* **12**, 1026–1039 (2017).
[4] N. Somaschi *et al.*, “Near-optimal single-photon sources in the solid state,” *Nat. Photon.* **10**, 340–345 (2016).
[5] D. Huber, M. Reindl, Y. Huo, H. Huang, J. S. Wildmann,

O. G. Schmidt, A. Rastelli, and R. Trotta, “Highly indistinguishable and strongly entangled photons from symmetric GaAs quantum dots,” *Nat. Commun.* **8**, 15506 (2017).
[6] D. Huber, M. Reindl, S. F. P. da Silva, C. Schimpf, J. Martín-Sánchez, H. Huang, G. Piredda, J. Edlinger, A. Rastelli, and R. Trotta, “Strain-Tunable GaAs Quantum Dot: A Nearly Dephasing-Free Source of Entangled Photon Pairs on Demand,” *Phys. Rev. Lett.* **121**, 033902 (2018).
[7] B. R. Mollow, “Power spectrum of light scattered by two-level systems,” *Phys. Rev.* **188**, 1699 (1969).
[8] A. Muller, E. B. Flagg, P. Bianucci, X. Y. Wang, D. G. Deppe, W. Ma, J. Zhang, G. J. Salamo, M. Xiao, and C. K. Shih, “Resonance fluorescence from a coherently driven semiconductor quantum dot in a cavity,” *Phys. Rev. Lett.* **99**, 187402 (2007).

- [9] C. Dory, K. A. Fischer, K. Müller, K. G. Lagoudakis, T. Sarmiento, A. Rundquist, J. L. Zhang, Y. Kelaita, and J. Vučković, “Complete Coherent Control of a Quantum Dot Strongly Coupled to a Nanocavity,” *Sci. Rep.* **6**, 25172 (2016).
- [10] H. Jayakumar, A. Predojević, T. Huber, T. Kauten, G. S. Solomon, and G. Weihs, “Deterministic Photon Pairs and Coherent Optical Control of a Single Quantum Dot,” *Phys. Rev. Lett.* **110**, 135505 (2013).
- [11] X. Xu, B. Sun, P. R. Berman, D. G. Steel, A. S. Bracker, D. Gammon, and L. J. Sham, “Coherent Optical Spectroscopy of a Strongly Driven Quantum Dot,” *Science* **317**, 929–932 (2007).
- [12] A. Ulhaq, S. Weiler, S. M. Ulrich, R. Rosßbach M. Jetter, and P. Michler, “Cascaded single-photon emission from the Mollow triplet sidebands of a quantum dot,” *Nat. Photon.* **6**, 238242 (2012).
- [13] B. Gao, G.-X. Li, and Z. Ficek, “Engineering a squeezed phonon reservoir with a bichromatic driving of a quantum dot,” *Phys. Rev. A* **94**, 033854 (2016).
- [14] Y. He, Y.-M. He, J. Liu, Y.-J. Wie, H. Y. Ramírez, M. Atature, C. Schneider, M. Kamp, S. Höfling, C.-Y. Lu, and J.-W. Pan, “Dynamically Controlled Resonance Fluorescence Spectra from a Doubly Dressed Single InGaAs Quantum Dot,” *Phys. Rev. Lett.* **114**, 097402 (2015).
- [15] F.-L. Li and S.-Y. Zhu, “Resonance fluorescence quenching and spectral line narrowing via quantum interference in a four-level atom driven by two coherent fields,” *Phys. Rev. A* **59**, 2330 (1999).
- [16] M. Peiris, K. Konthasinghe, Y. Yu, Z. C. Niu, and A. Muller, “Bichromatic resonant light scattering from a quantum dot,” *Phys. Rev. B* **89**, 155305 (2014).
- [17] F. Grossmann, T. Dittrich, P. Jung, P. Hänggi, “Coherent Destruction of Tunneling,” *Phys. Rev. Lett.* **67**, 516 (1991).
- [18] K. M. Fonseca-Romero, S. Kohler, P. Hänggi, “Coherence Stabilization of a Two-Qubit Gate by ac Fields,” *Phys. Rev. Lett.* **95**, 140502 (2005).
- [19] X. Xu, Z. Wang, C. Duan, P. Huang, P. Wang, Y. Wang, N. Xu, X. Kong, F. Shi, X. Rong, J. Du, “Coherence-Protected Quantum Gate by Continuous Dynamical Decoupling in Diamond,” *Phys. Rev. Lett.* **109**, 070502 (2012).
- [20] G. S. Agarwal, Y. Zhu, D. J. Gauthier, and T. W. Mossberg, “Spectrum of radiation from two-level atom under intense bichromatic excitation,” *J. Opt. Soc. Am. B* **8**, 1163 (1991).
- [21] Z. Ficek, and H. S. Freedhoff, “Resonance-fluorescence and absorption spectra of a two-level atom driven by a strong bichromatic field,” *Phys. Rev. A* **48**, 3092 (1993).
- [22] A. Papageorge, A. Majumdar, E. D. Kim, and J. Vučković, “Bichromatic driving of a solid-state cavity quantum electrodynamics system,” *New J. Phys.* **14**, 013028 (2012).
- [23] Z. Ficek, and H. S. Freedhoff, “Fluorescence and absorption by a two-level atom in a bichromatic field with one strong and one weak component,” *Phys. Rev. A* **53**, 4275 (1996).
- [24] B. Blind, P. R. Fontana, P. Thomann, “Resonance fluorescence spectrum of intense amplitude modulated laser light,” *J. Phys. B: At. Mol. Phys.* **13**, 2717 (1980).
- [25] M. Maragkou, C. Sánchez-Muñoz, S. Lazić, E. Chernysheva, H. P. van der Meulen, A. González-Tudela, C. Tejedor, L. J. Martínez, I. Prieto, P. A. Postigo, and J. M. Calleja, “Bichromatic dressing of a quantum dot detected by a remote second quantum dot,” *Phys. Rev. B* **88**, 075309 (2013).
- [26] Y. Zhu, Q. Wu, A. Lezama, D. J. Gauthier, and T. W. Mossberg, “Resonance fluorescence of two-level atoms under strong bichromatic excitation,” *Phys. Rev. A* **41**, 6574(R) (1990).
- [27] C. C. Yu, J. R. Bochinski, T. M. V. Kordich, T. W. Mossberg, and Z. Ficek, “Driving the driven atom: Spectral signatures,” *Phys. Rev. A* **56**, R4381(R) (1997).
- [28] J. Pan, H. Z. Jooya, G. Sun, Y. Fan, P. Wu, D. A. Telnov, S.-I. Chu, and S. Han, “Absorption spectra of superconducting qubits driven by bichromatic microwave fields,” *Phys. Rev. B* **96**, 174518 (2017).
- [29] T. Rudolph, H. S. Freedhoff, and Z. Ficek, “Shift of the subharmonic resonances and suppression of fluorescence in a two-level atom driven by a bichromatic field,” *J. Opt. Soc. Am. B* **15**, 2325 (1998).
- [30] C. Gustin, R. Manson, and S. Hughes, “Spectral asymmetries in the resonance fluorescence of two-level systems under pulsed excitation,” *Opt. Lett.* **43**, 779 (2018).
- [31] A. V. Kuhlmann, J. Houel, A. Ludwig, L. Greuter, D. Reuter, A. D. Wieck, M. Poggio, and R. J. Warburton, “Charge noise and spin noise in a semiconductor quantum device,” *Nat. Phys.* **9**, 570 (2013).
- [32] A. Nazir and D. P. S. McCutcheon, “Modelling exciton-phonon interactions in optically driven quantum dots,” *J. Phys. Condens. Matter* **28**, 103002 (2016).
- [33] A. J. Ramsay, A. V. Gopal, E. M. Gauger, A. Nazir, B. W. Lovett, A. M. Fox, and M. S. Skolnick, “Damping of exciton Rabi rotations by acoustic phonons in optically excited InGaAs/GaAs quantum dots,” *Phys. Rev. Lett.* **104**, 017402 (2010).
- [34] B. Krummheuer, V. M. Axt, and T. Kuhn, “Theory of pure dephasing and the resulting absorption line shape in semiconductor quantum dots,” *Phys. Rev. B* **65**, 195313 (2002).
- [35] L. Besombes, K. Kheng, L. Marsal, and H. Mariette, “Acoustic phonon broadening mechanism in single quantum dot emission,” *Phys. Rev. B* **63**, 155307 (2001).
- [36] J. Förstner, C. Weber, J. Danckwerts, and A. Knorr, “Phonon-assisted damping of Rabi oscillations in semiconductor quantum dots,” *Phys. Rev. Lett.* **91**, 127401 (2003).
- [37] C. Roy and S. Hughes, “Phonon-Dressed Mollow Triplet in the Regime of Cavity Quantum Electrodynamics: Excitation-Induced Dephasing and Nonperturbative Cavity Feeding Effects,” *Phys. Rev. Lett.* **106**, 247403 (2011).
- [38] A. Ulhaq, S. Weiler, C. Roy, S. M. Ulrich, M. Jetter, S. Hughes, and P. Michler, “Detuning-dependent Mollow triplet of a coherently-driven single quantum dot,” *Optics Express* **21**, 4382 (2013).
- [39] A. Nazir, “Photon statistics from a resonantly driven quantum dot,” *Phys. Rev. B* **78**, 153309 (2008).
- [40] D. P. S. McCutcheon, and A. Nazir, “Quantum dot Rabi rotations beyond the weak exciton-phonon coupling regime,” *New J. Phys.* **12**, 113042 (2010).
- [41] C. Gustin, and S. Hughes, “Pulsed excitation dynamics in quantum-dot-cavity systems: Limits to optimizing the fidelity of on-demand single-photon sources,” *Phys. Rev. B* **98**, 045309 (2018).
- [42] D. L. Aronstein, R. S. Bennink, R. W. Boyd, C. R. Stroud, Jr., “Comment on Resonance-fluorescence and

- absorption spectra of a two-level atom driven by a strong bichromatic field,” *Phys. Rev. A* **65**, 067401 (2002).
- [43] D. J. Tannor, *Introduction to Quantum Mechanics: A Time-Dependent Perspective* (University Science Books, 2007).
- [44] J. H. Shirley, “Solution of the Schrödinger Equation with a Hamiltonian Periodic in Time,” *Phys. Rev.* **138**, B979 (1965).
- [45] H-P. Breuer, and F. Petruccione, *The Theory of Open Quantum Systems* (Oxford University Press, New York, 2002).
- [46] R J Warburton, C. Schäflein, D Haft, F Bickel, A Lorke, K Karrai, J M Garcia, W Schoenfeld, and P M Petroff, “Optical emission from a charge-tunable quantum ring,” *Nature* **405**, 926–929 (2000).
- [47] P. W. Fry, I. E. Itskevich, D. J. Mowbray, M. S. Skolnick, J. J. Finley, J. A. Barker, E. P. O’Reilly, L. R. Wilson, I. A. Larkin, P. A. Maksym, M. Hopkinson, M. Al-Khafaji, J. P.R. David, A. G. Cullis, G. Hill, and J. C. Clark, “Inverted Electron-Hole Alignment in InAs-GaAs Self-Assembled Quantum Dots,” *Physical Review Letters* **84**, 733–736 (2000).
- [48] Andreas V. Kuhlmann, Julien Houel, Daniel Brunner, Arne Ludwig, Dirk Reuter, Andreas D. Wieck, and Richard J. Warburton, “A dark-field microscope for background-free detection of resonance fluorescence from single semiconductor quantum dots operating in a set-and-forget mode,” *Review of Scientific Instruments* **84**, 073905 (2013).
- [49] M. Bayer, G. Ortner, O. Stern, A. Kuther, A. A. Gorbunov, A. Forchel, P. Hawrylak, S. Fafard, K. Hinzer, T. L. Reinecke, S. N. Walck, J. P. Reithmaier, F. Klopff, and F. Schäfer, “Fine structure of neutral and charged excitons in self-assembled In(Ga)As/(Al)GaAs quantum dots,” *Phys. Rev. B* **65**, 195315 (2002).
- [50] S. Weiler, A. Ulhaq, S. M. Ulrich, D. Richter, M. Jetter, P. Michler, C. Roy, and S. Hughes, “Phonon-assisted incoherent excitation of a quantum dot and its emission properties,” *Phys. Rev. B* **86**, 241304(R) (2012).
- [51] C. Roy and S. Hughes, “Polaron master equation theory of the quantum-dot Mollow triplet in a semiconductor cavity-QED system,” *Phys. Rev. B* **85**, 115309 (2012).